International Journal of Biological Macromolecules 260 (2024) 129452

Contents lists available at ScienceDirect

International Journal of Biological Macromolecules

journal homepage: www.elsevier.com/locate/ijbiomac

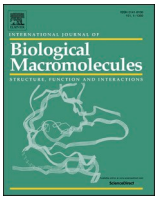

Phasor-FLIM analysis of cellulose paper ageing mechanism with carbotrace 680 dye

Vittorio Ferrara [a], Valeria Vetri [a], Bruno Pignataro [a], Delia Francesca Chillura Martino [b,*], Giuseppe Sancataldo [a,*]

[a] Department of Physics and Chemistry - Emilio Segrè, University of Palermo, viale delle Scienze, Palermo 90128, Italy
[b] Department of Biological, Chemical and Pharmaceutical Sciences (STeBiCeF), University of Palermo, viale delle Scienze, Palermo 90128, Italy

ARTICLE INFO

Keywords:
Paper ageing
Fluorescence-lifetime imaging microscopy
Carbotrace dye
Cellulose oxidation
Paper crystallinity

ABSTRACT

Ageing of paper is a complex process of great relevance for application purposes because of its widespread use as support for information storage in books and documents, and as common low-cost and green packaging material, to name a few. A key factor in paper ageing is the oxidation of cellulose, a macromolecule of natural origin that constitutes the main chemical component of paper. Such a complex process results in changes in the cellulose polymeric chains in chemical and structural properties. The scope of this work is to explore the effects of oxidation of cellulose as one of the principal mechanisms of ageing of paper using a fluorescence-based approach. To this aim, fluorescence-lifetime imaging microscopy (FLIM) measurements on pure cellulose samples stained using Carbotrace 680 dye were performed, and data were analyzed by phasor approach. The comparison with results from conventional techniques allowed to map paper microstructure as a function of the sample oxidation degree correlating the fluorescence-lifetime changes to cellulose oxidation. A two-step oxidation kinetics that produced specific modification in paper organization was highlighted indicating that FLIM measurements using Carbotrace 680 dye may provide a simple tool to obtain information on the oxidation process also adding spatial information at sub-micrometric scale.

1. Introduction

Paper is one of the most important materials currently used for many applications, such as low-cost and green packaging for food, [1] electrical insulation in cables and power transformers, [2] decorative and smart component in buildings interior as wallpaper. [3] However, the likely most prominent role paper has played for human activities worldwide is as common support to make manuscripts, archival documents, books, and artistic works. In fact, since the 2nd century AC, paper has affirmed its role from the historical and artistic point of view as information carrier, and support for many graphical arts. [4,5]

Chemically, paper is a complex multi-component material of natural origin mainly constituted of cellulose. Cellulose is the most abundant natural biopolymer on the Earth with a yield of about 1.5×10^{12} tons per year, currently obtained from a wide range of sources, such as plants, algae, and bacteria. [6–8] It is a linear homopolymer of D-glucose linked through 1,4-β-glucosidic bond, naturally occurring as polymeric microfibrils in a semi-crystalline state. [9,10]

It is well assessed that properties of paper (e.g. straightness, durability, color) are affected by the content of cellulose and its chemical integrity. [11] Cellulose may be subjected to many deterioration mechanisms due to chemical, physical, and biological factors as it is sensitive to temperature and light, as well as to the enzymatic activity of cellulolytic microorganisms that can colonize its surface. [12,13]

Among the chemical degradative processes, oxidation and hydrolysis of cellulose chains are recognized as the main degradation patterns occurring in the paper under common conditions of storage.

Oxidation mainly results in loss of paper strength and yellowing as a consequence of the formation of carbonyl groups and the formation of carbonyl conjugated double bonds, while hydrolysis induces cellulose chains depolymerization and breaking resulting in a more fragile material. [14,15] Cellulose oxidation and hydrolysis reactions are currently the subject of diverse studies because of the almost ubiquitous presence of water and oxygen in the atmosphere affecting shelf-life and applicability of cellulosic materials. [16,17]

Such degradation processes are slow but induce relevant

* Corresponding authors.
E-mail addresses: delia.chilluramartino@unipa.it (D.F. Chillura Martino), giuseppe.sancataldo@unipa.it (G. Sancataldo).

https://doi.org/10.1016/j.ijbiomac.2024.129452
Received 3 November 2023; Received in revised form 5 January 2024; Accepted 10 January 2024
Available online 14 January 2024

modifications on the cellulose fibers over time that clearly represent a relevant issue, especially in the field of Cultural Heritage, since ancient paper-based items have to be preserved for long time to avoid deterioration.

Several efforts have been made for a more detailed characterization of the intrinsic proprieties of cellulose, as well as, for a better comprehension of its ageing mechanisms. [18–20] A typical approach to investigate the effects of ageing on paper and other cellulosic materials consists in inducing artificial accelerated ageing which is an efficient and useful methodological strategy for studying cellulose and paper degradation since natural ageing can take many years to several decades to produce statistically significant changes. [21] The ageing in paper samples is commonly induced through the use of chemical oxidizing agents under controlled experimental conditions. Salts of meta-periodate ion (IO_4^-) in aqueous solution are the most used compounds to oxidize paper, through the Malaprade reaction, as it reacts with cellulose to yield the oxidized derivative known as dialdehyde cellulose. [22] The oxidation reaction of cellulose with IO_4^- is widely used as it is characterized by high selectivity. [23] In fact, the oxidation with meta-periodate causes a selective cleavage of the C2-C3 bond in the anhydroglucose units of cellulose due to the oxidation of the related secondary hydroxyls to a couple of aldehydic carbonyl groups. The high selectivity is due to the oxidation mechanism which requires vicinal hydroxyls, as such groups are located at the C2 and C3 positions. [24] Thus, the oxidation reaction proceeds via the formation of a cyclic diester of meta-periodate ion with vicinal hydroxyls, that subsequently undergoes an intramolecular redox process with C—C bond cleavage according to the concerted mechanism of the Malaprade reaction, with no significant side reactions nor further oxidation to carboxyl groups. [24,25]

By the use of this strategy, the ageing of paper made of pure cellulose has been investigated by mainly quantifying the most relevant parameters such as carbonyl content upon oxidation, paper acidification, decrease of the degree of polymerization, deterioration of the mechanical properties, and changes in crystallinity. These physicochemical modifications at the level of cellulose chains chemistry and structural arrangement determine a loss of mechanical strength, whiteness, and usability of paper at the macroscopic scale. [4,24,26–28]

Even though the extensive ageing of cellulose is well-known to induce a net decrease of polymeric chain length, breaking of hydrogen bonds, and a lowering of crystallinity degree, the process which leads to such effects has been suggested not to be monotonic. Intriguingly, some studies about the oxidation of pure cellulose paper have found a two-step mechanism, involving principally the oxidation of the more exposed and accessible amorphous portions of cellulose in the first phase of the process, then the oxidative attack to the more packed crystalline regions. [24,29] In particular, a two-step process has been suggested by analyses typically applied for polymeric structures characterization, such as X-ray diffraction (XRD) and differential scanning calorimetry (DSC). [29] These techniques have shown changes in crystallinity and decomposition temperature for cotton cellulose upon oxidation, and allowed evidence that crystallinity slightly increased at the beginning of the process, then decreased as a function of the oxidation of time.

The advantageous characteristics of fluorescence techniques, such as low molecular detection limits and high sensitivity to physicochemical changes in the fluorophore environment, have been exploited to study paper properties and oxidation, as well. For instance, fluorescence measurements have been applied to investigate the properties of paper and other more complex cellulose-based systems, such as composites with synthetic polymers, ancient artefacts, and biological structures. [30–33] Concerning the oxidation of paper, fluorescence has enabled obtaining data about the oxidation mechanism through the fluorolabelling free carbonyls of cellulose with carbazole carbonyl oxyamine dye. [24,34,35] The selective fluorolabelling of carbonyl groups in the highly ordered crystalline regions of cellulose has also confirmed two distinct phases for the oxidation process by meta-periodate ion. [24] Yet, this effective approach is based on a chemical reaction carried out through a protocol for the carbonyl functions to be fluorolabelled, followed by sample purification. In addition, the main limit to evaluate the oxidation degree of cellulose by the detection of the carbonyl groups is represented by the intra- and inter-chain crosslinking reactions. In fact, only the free carbonyl groups can be detected, while a fraction of these groups can be masked as hemiacetals formed by reaction with adjacent cellulose hydroxyls, leading to an underestimate of the actual amount of oxidized functions. [36]

In the present work, an advantageous strategy to monitor the cellulose oxidation in paper samples overcoming some limitations of the previously reported approaches is presented. By exploiting the properties of Carbotrace 680 fluorescent dye, and using fluorescence lifetime imaging microscopy (FLIM) combined with a phasor approach, the modifications induced by oxidation of cellulose fibers in paper were mapped at the sub-micrometric scale.

Carbotrace 680 is a recently developed fluorescent short length anionic oligothiophene, that selectively binds glucans. [37] It is characterized by a central heterocyclic benzodithiazole motif, and an intrinsic donor–acceptor–donor electronic structure, that makes it a fluorescent dye with improved spectral properties compared to previously reported oligothiophenes, due to the possibility of intramolecular charge transfer transitions. This dye has been shown to present different spectral properties when bound to different stereoisomers allowing, for example, to discriminate between starch and cellulose in potato tissue using confocal fluorescence microscopy. [37]

The effects of oxidation induced by the Malaprade reaction on cellulose paper samples were first analyzed by means of well-affirmed techniques for cellulosic materials characterization, such as pH measurements, X-ray diffraction (XRD) and attenuated total reflectance Fourier transform infrared spectroscopy (ATR-FTIR). The paper samples were then characterized by fluorescence confocal microscopy through steady-state and time-resolved fluorescence intensity measurements after staining with Carbotrace 680. The FLIM-based approach is demonstrated to represent a powerful tool for studying the paper properties upon oxidation. Indeed, FLIM offers a way to exploit fluorescence lifetime measurements as a parameter to investigate the chemical and structural state of cellulose in paper. [38–41] Also, FLIM allows the possibility to map fluorescence lifetime at the micro- and nanometric scale to obtain images, [42–47] which encode information about the spatial distribution of the dye in the stained paper, along with information about the environment the dye experiences as bound to the paper fibers. [48] FLIM data were analyzed by means of a phasor approach, which consists of a model-free method that enables to easily visualize fluorescence lifetime distribution of the observed image at pixel resolution. [41,49] The phasor approach to fluorescence lifetime imaging has emerged as a widely adopted technique for dissecting intricate fluorescence signals. The phasor representation of complex fluorescence decays offers a compelling advantage, providing a graphical depiction of entire sample decays allowing a straightforward visualization and interpretation of data. Notably, the phasor approach transforms complex fluorescence decays without resorting to fitting models, ensuring that it retains the same information content as the original data. The resultant phasor plot is distinctive to a specific system, exhibiting high reproducibility and serving as a robust means to assess the presence of molecular interactions. Recent advancements have enabled the quantification of multiple components from phasor plots in fluorescence lifetime imaging microscopy. This capability surpasses the current limitations of data fitting methods, particularly in the context of biomolecular systems, where such comprehensive quantification was not previously achievable. [50–52] Then, the analysis and comparison of the obtained data from the kinetic studies of the paper oxidation reveals a two-steps mechanism, suggesting that the Malaprade reaction firstly involves the cellulose amorphous phase, then the more packed crystalline regions.

Therefore, the phasor-FLIM analysis of paper oxidation by staining

with Carbotrace 680 enabled an advantageous and effective in-depth investigation of the effects of accelerated ageing on pure cellulose paper, with a detailed view of the kinetics steps characteristic of the cellulose oxidation process. The method represents a valuable tool to investigate the ageing mechanism of cellulose microstructures with the possibility to extend the approach to other degradative mechanisms, as well as to the ageing of other more complex cellulose-based systems.

2. Experimental section

2.1. Paper oxidation and pH measurements

The pure cellulose paper samples used for the experiments were Whatman no. 1 lab filters. This type of paper is obtained from cotton linters and is constituted of pure cellulose. [53] For the oxidation process through the Malaprade reaction, a paper filter of ~0.5 g was soaked in 50 mL of 15 mM potassium meta-periodate (KIO_4, 99.8 %, Sigma Aldrich) aqueous solution at different times. Then, the paper filter was thoroughly rinsed with deionized water and let spontaneously dry overnight. All the steps were carried out at room temperature in the dark. For each oxidized sample, non-destructive surface pH measurements were carried out using a Hanna Instruments pH 211 pH meter equipped with a flat electrode according to the T 529 om-04 TAPPI method.

2.2. Carbonyl content determination

The carbonyl content was measured through the colorimetric TTC (triphenyl tetrazolium chloride) assay. [26,54] The TTC assay is based on the redox reaction between the free carbonyl groups of the oxidized cellulose in paper with 2,3,5-triphenyltetrazolium chloride (TTC, 98.0 %, Sigma Aldrich) in an alkaline medium. Briefly, 30 mg of paper cut into small pieces were put in a 10 mL glass tube, then 0.5 mL of KOH 0.2 M and 0.5 mL of TTC 0.2%*w/v* aqueous solutions were added. The reaction was carried out in a water bath at 70 °C for 10 min in the dark. After cooling in an ice bath, 0.2 mL of aqueous HCl 1 M were added to block the reaction. The red precipitate, that is triphenylformazane yielded by the TTC reduction, was solubilized with ethanol to a final volume of 10 mL, and its concentration was evaluated by UV–Vis absorption spectroscopy by a UV–Vis-NIR V-770 Jasco spectrophotometer. Spectra were recorded in a 1.00 cm quartz cuvette in the range 200–800 nm, with a bandwidth of 2.0 nm, and a scan speed of 200 nm/min. The absorbance values at $\lambda = 485$ nm enabled to calculate the carbonyl content by the use of a calibration curve obtained with a standard aqueous solution of glucose. [54]

2.3. Crystallinity measurements

The crystallinity of paper samples at different oxidation degrees was measured by XRD and ATR-FTIR measurements. The XRD patterns were collected through a Bruker ecoD8 ADVANCE (Bruker, Billerica, MA, USA) spectrometer working in the θ-2θ geometry equipped with a Cobalt tube (Co; $\lambda = 1.79$ Å) and a LYNEXEYE (1D mode) detector operating at 40 kV and 25 mA. XRD patterns were recorded in the 5.0°–70.0° (2θ) range with a 1 mm window, an increment of 0.0198°, and time per step of 1.00 s. The XRD data were analyzed by Match! 3 software.

ATR-FTIR spectra were collected by using an FTIR Bruker Vertex Advanced Research Fourier Transform Infrared spectrometer (Bruker, Billerica, MA, USA) equipped with a Platinum ATR and a diamond crystal, in the 70–4000 cm^{-1} range, spectral resolution of 2 cm^{-1} and 200 scans. FTIR spectra were analyzed by using OPUS (7.5) software.

2.4. Fluorescence confocal microscopy and FLIM measurements

Paper was stained by soaking the sample (5 mg) in 100 μL of 4 μg/mL Carbotrace 680 (Ebba Biotech, Sweden) aqueous solution for 2 h. The paper samples were kept wet for the fluorescence analyses. Steady-state and time-resolved fluorescence intensity measurements were both carried out by using a Leica TSC SP5 confocal laser scanning microscope, with a 63×, 1.4 NA oil objective (Leica Microsystems, Wetzlar, Germany). Fluorescence spectral imaging was performed acquiring 512 × 512-pixels images using $\lambda_{exc} = 550$ nm in the range 580–780 nm with a 20 nm bandwidth.

FLIM measurements were collected in the time domain using the Leica TCS SP5 inverted microscope coupled with a PicoHarp 300 TCSPC Module (PicoQuant, Berlin, Germany). 256 × 256 pixels FLIM measurements were obtained by setting the fluorescence acquisition range 580–780 nm and $\lambda_{exc} = 550$ nm from a white light laser with a repetition rate of 80 MHz (Leica Microsystem).

2.5. FLIM phasor plot analysis and interpretation

FLIM data were analyzed by using the phasor approach. [52] This is a Fourier domain technique that allows the transformation of the signal from each pixel of the image to a single point, namely phasor, on a polar plot commonly called “universal circle”. In this representation, all possible single-exponential decays measured at each pixel of the image are transformed to points lying on a semicircle, with radius 1/2, going from point (0,0), corresponding to an infinite lifetime, to point (1,0), corresponding to lifetime of 0. Complex decays typically lie within the universal circle. Each pixel in the FLIM image corresponds to a single pixel in the phasor plot, then by using colored cursors it is possible to select pixels in the phasor plot so that the corresponding pixels in the measurement appear colored accordingly generating the so-called lifetime maps. [41] For more complex exponential decays, the phasors appear inside the universal circle. In the case of a double exponential decay, since phasors follow the rules of vector algebra, measured lifetimes are located along a straight line joining the phasors of the two main lifetime components and it is possible to geometrically resolve the fractions of single decay components by the lever rule. [41,52] By calculating the fraction of each lifetime single component, that is proportional to the distance of the phasor from the other pure component, it is possible to obtain lifetime fraction maps.

In this work, FLIM data were processed using SimFCS4 software (Laboratory for Fluorescence Dynamics, University of California, Irvine, CA, available at www.lfd.uci.edu), and fraction maps were obtained using a double exponential model. The dye Alexa Fluor 594 in aqueous solution, characterized by a single exponential decay and a lifetime of 3.9 ns, was used for calibration.

3. Results and discussion

Cellulose oxidation process is fundamental in determining the macroscopic properties of paper. Monitoring physical and chemical parameters, such as pH, carbonyl content and crystallinity is crucial to define the ageing degree of paper. In the following the effects of the ageing on the main physicochemical features of pure cellulose paper were determined during oxidation by means of well-affirmed techniques for paper analysis, as well as by phasor-FLIM measurements on Carbotrace 680 stained samples.

3.1. Acidity measurements

Cellulose paper was oxidized by incubating samples in 15 mM KIO_4 at different time intervals. The pH of each sample was measured at specific time points by a non-destructive protocol using a flat electrode after removing the oxidizing agent by washing with Milli-Q water. In Fig. 1, the pH of the different samples oxidized for specific time intervals is reported up to 1440 min (24 h). As can be seen, starting from a pH value nearly neutral a decrease of pH is measured as a function of the treatment time. The higher measured pH value, before treatment ($t = 0$), is compatible with the one expected for a pure cellulose sample such as

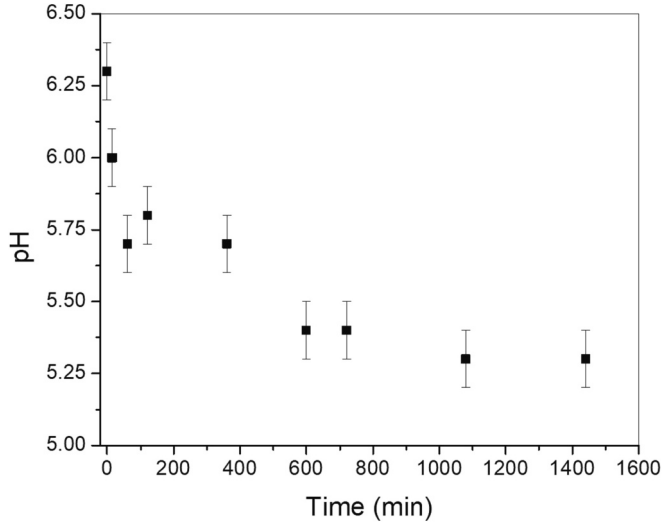

Fig. 1. pH values of pure cellulose paper samples incubated in 15 mM KIO4 for different time intervals. Measured pH decay is ascribed to increased oxidation level of the samples.

Whatman no.1, and the lowering of pH can be ascribed to increasing oxidation. [55] The decrease of pH from pH = 6.3 ± 0.1 to pH = 5.3 ± 0.1 is observed, and a stable value is reached in about 600 min. The oxidation process of paper is known to lower its pH, and this measurement is routinely used as a marker of cellulose oxidation [55,56] so that the lowering of pH is taken into account as an indication that the Malaprade reaction was successfully applied to the samples.

3.2. Carbonyl content

The ageing of cellulose in paper samples determines an increase in the carbonyl content as a result of the oxidation of hydroxyl groups. Therefore, monitoring the carbonyl content as a function of the oxidation time is a common way to confirm the oxidation of cellulose and follow the extent of such a chemical modification over time. [54] The Malaprade reaction is widely used to induce accelerated ageing of paper as it is effective in inducing the formation of carbonyl groups upon specific homolytic scission of the 2C—3C bond at the anhydroglucose units on the cellulose chains. [24,25] To determine the carbonyl content, which is indicative of the degree of oxidation of cellulose, the TTC assay is commonly applied. The TTC assay is a redox colorimetric method which consists in the oxidation of free carbonyl groups of the cellulose structure, and the concomitant reduction of the 2,3,5-triphenyltetrazolium chloride salt to 1,3,5-triphenyl-tetrazolium formazan (triphenylformazan). The typical red color of triphenylformazane is detected by UV–Vis absorption spectroscopy at λ = 485 nm for the carbonyl content estimation. [54] Fig. 2 reports the results of the TTC assay carried out for cellulose paper samples at different oxidation times up to 1440 min (24 h).

In Fig. 2A, the UV–Vis absorption spectra of triphenylformazan in alcoholic solution obtained treating oxidized paper samples at different extents of oxidation are reported, showing the typical absorption maximum at λ = 485 nm along with a secondary component at λ = 528 nm. Upon the oxidation process, the carbonyl content is expected to increase, as demonstrated by the raising of the intensity of triphenylformazan absorption spectra as a function of oxidation time. In order to quantify the amount of free carbonyl groups, the absorbance value at λ = 485 nm was evaluated for the calculation by using a calibration curve obtained from glucose standard solutions. In Fig. 2B, the carbonyl fraction is reported as a function of the oxidation time. As can be seen, a monotonic growth of carbonyl fraction which reaches a plateau after 900 min of incubation occurs.

3.3. Crystallinity analyses

Crystallinity of cellulose is a fundamental characteristic to determine and control because of the effects this property determines the utilisation of paper, as well as to monitor its conservation state. In fact, it is well-known that the crystallinity degree of cellulose lowers over time as a consequence of the paper ageing mechanisms. Many approaches have been developed to calculate the crystallinity index parameter of cellulose in paper samples from quantitative measurements, typically based on X-ray diffraction (XRD), and Fourier transform infrared spectroscopy (FTIR) techniques. [27,57]

Here, both XRD and ATR-FTIR techniques were applied to monitor the crystallinity changes in paper samples upon the oxidation process induced by the Malaprade reaction, and the results are reported in Fig. 3. In Fig. 3A, the values of the Crystallinity Index (CI) from XRD measurements for oxidized paper samples up to 1440 min (24 h) are reported as a function of the reaction time.

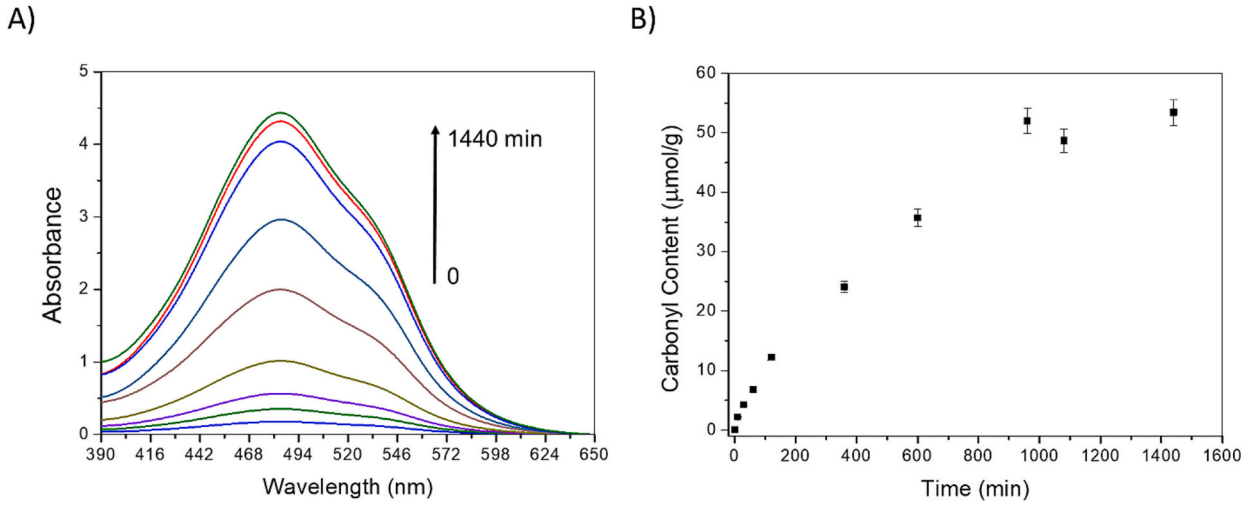

Fig. 2. TTC assay for samples of cellulose paper oxidized at different time points up to 1440 min (24 h): A) UV–Vis absorption spectra in the range 390–650 nm of the triphenylformazan in alcoholic solution yielded by the redox reaction with free carbonyl groups present in the oxidized cellulose of paper (each spectrum was acquired at absorbance less than 1, then multiplied by the dilution factor), and B) quantification of the amount of carbonyl groups (µmol of carbonyl groups per gram of paper) at different oxidation times.

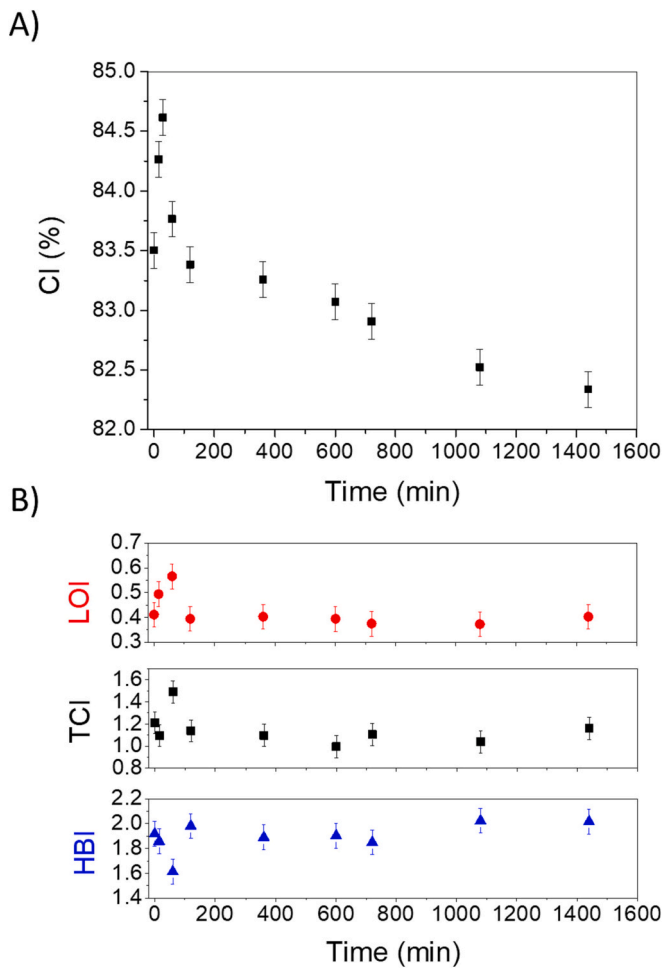

Fig. 3. Crystallinity analysis of pure cellulose paper upon oxidation at different time points up to 1440 min (24 h): A) Crystallinity Index (CI) calculated by the Segal method [28] from the height of the XRD diffraction peak, and B) values of the crystallinity parameters LOI, TCI, and HBI, calculated from the intensity of proper ATR-FTIR absorption bands as follows: LOI = 1429 cm^{-1}/893 cm^{-1} (red), TCI = 1370 cm^{-1}/2900 cm^{-1} (black), and HBI = 3332 cm^{-1}/1336 cm^{-1} (blue).

By the use of the XRD pattern, it is possible to measure the CI by using the Segal method. [28,58] The Segal method permits calculation of CI from the XRD diffractograms of cellulose samples as the ratio of the height of the peak 200 (I_{200}) and the height of the minimum (I_{AM}) between the peaks 200 and the 110 (Fig. S1). The CI is widely used to interpret changes in cellulose structure after physicochemical treatments and gives a quantitative estimation of sample crystallinity which results to be 83.5 % for Whatman paper samples before treatment, in agreement with commonly reported values calculated by XRD measurements. [27,59]

As shown, at the initial stages of the oxidizing treatment, an increase of CI to 84.6 % was observed at 30 min, followed by a progressive decrease of the crystallinity over time reaching CI of 82.4 % at 1440 min, which is lower than the initial value for the untreated paper. The observed trend can be explained as a consequence of a two-step kinetic mechanism of paper oxidation in accordance with previously reported results, which is usually related to the semi-crystalline nature of cellulose. [24,29]

The oxidation process is supposed to firstly affect the amorphous phase of cellulose, constituted of less dense and more exposed polysaccharide chains. This step is also associated with a breaking and depolymerization of the cellulose polymeric chains, which degrade the amorphous regions at the beginning of the process, by leading to the initial apparent increase of crystallinity. As the oxidation of the amorphous regions proceeds, the oxidation of the crystalline portion of cellulose starts to occur as well, and the CI can decrease over time.

To gain more information about changes in paper crystallinity upon oxidation, samples were investigated also by means of ATR-FTIR spectroscopy. By the use of ATR-FTIR spectroscopy, it was possible to follow modifications in the packing of cellulose chains in more detail by evaluating the ratio between the intensity of characteristic peaks, associated with specific chemical groups. Such chemical groups are typically involved in inter- and intramolecular weak bonds in cellulose crystalline structures, so that changes in their intensity can be associated with structural rearrangement of the polymeric chains. Then, these measurements lead to a more detailed view of the oxidation effects on the polymer chain assembly, which affects the overall cellulose crystallinity. In particular, in Fig. 3B the *lateral order index* (LOI), the *total crystallinity index* (TCI), and the *hydrogen-bond intensity* (HBI) are reported. These parameters have been widely applied to cellulose structural studies. [60–62] The LOI is related to the weak bonds the C6 forms in the structure of different types of cellulose polymorphs, and is calculated as the ratio of the intensity of bands 1429 cm^{-1}/893 cm^{-1}, as the signal at 1429 cm^{-1}, attributed to -CH_2- symmetric bending or scissoring motion, is known to be very sensitive to changes of conformation, while the band at 893 cm^{-1} attributed to the β-(1,4) glyosidic bond vibrations is almost unaffected by allomorphic transformations or loss of crystallinity. [60] Calculations of TCI were performed from the ratio of the absorption bands at 1370 cm^{-1}/2900 cm^{-1}. TCI is an experimental parameter obtained by the ratio of a band sensitive to crystallinity changes, such as 1370 cm^{-1} assigned to the -CH- bending, and the band at 2900 cm^{-1} related to the -CH- stretching. [63] In both cases, the use of a ratio of bands intensity, instead of monitoring a single band, provides a kind of internal standard to compensate for the uncertainty sources of variations due to sample inhomogeneities, crystallites distribution, and extent of scattered light from one sample to another. [64] In addition, the HBI parameter was also calculated as the ratio 3332 cm^{-1}/1336 cm^{-1}, which corresponds to the -OH stretching and the -CH- rocking, respectively. The HBI parameter is closely related to the crystalline structure of cellulose and the degree of intermolecular regularity, as well as to the amount of bound water. The HBI value is lower for more packed crystalline structures as a consequence of less accessibility of the cellulose chains to the water molecules for interaction. [57,65]

The values of LOI, TCI, and HBI parameters were determined for the untreated paper and the paper oxidized at different reaction times. LOI and TCI values increase up to 60 min, then decrease to the initial value with no relevant modifications over time afterward. Their higher values in the first part of the kinetics can be related to the growth of the crystalline component, or equivalently to a partial loss of the amorphous component, of the sample upon oxidation. In the second step LOI and TCI lower back to their initial values as a consequence of the oxidation of the crystalline phase, due to the breaking of the weak bonds in which the -CH_2- and the -CH- are involved. In addition, the HBI trend is relevant too, since it can be useful to correlate the cellulose structure to the accessibility of the polymeric chains to the interaction with water molecules. [57,65] Also, for the HBI parameter the typical *mirror effect* is observed respect to LOI and TCI, insofar as where TCI and LOI exhibit a maximum, the HBI shows a minimum. [61] Then, the here reported initial HBI decrease up to 60 min can be related to a higher crystallinity, or again to a partial loss of the amorphous component which is typically more hydrated, as the lower degree of structure is associated with a higher accessibility to water molecules.

Comparing the data from XRD and ATR-FTIR analyses, the crystallinity parameters from ATR-FTIR change accordingly to the CI in the first part of the paper oxidation kinetics. Then, XRD detects a decrease in crystallinity that is not detected by ATR-FTIR, by which constant values for LOI, TCI and, HBI are observed in the second step of the oxidation process. This difference can be explained as XRD measures an overall change in crystallinity of the paper sample, meanwhile, by the

calculation of the crystallinity parameters from ATR-FTIR, the effects of the oxidation process on specific interactions in the cellulose structure are investigated. In both cases, a complete overview of the kinetics of the paper oxidation evidences that the process is characterized by two different steps, clearly distinguishable by these structural analyses. These results represent a further confirmation of the two-step mechanism of oxidation for cellulose in paper samples during the Malaprade reaction. The aforementioned mechanism by which the amorphous parts of the cellulose structure are firstly involved in the oxidation and depolymerization process can explain the observed results.

3.4. Steady-state fluorescence and phasor-FLIM analysis of paper oxidation

To gain further information about the effects of accelerated ageing, pure cellulose paper samples were fluorolabelled with Carbotrace 680 dye before and after the oxidation reaction, and analyzed by fluorescence confocal microscopy through steady-state and time-resolved fluorescence intensity measurements. The use of Carbotrace 680 as staining agent represents an advantageous aspect in the herein reported method, since the fluorolabelling can be easily carried out by simple dye physisorption on the paper fibers in an aqueous environment. No further purification protocol is required after labelling as the unbound dye does not emit in water. [37] This property is also observed for other environmentally sensitive dyes used to label biomolecular structures, [66,67] and represents a useful feature in staining protocols.

In Fig. 4A-B confocal images are shown and cellulose fibers, typical of paper, are clearly visible at the microscale in both untreated paper and sample oxidized for 1440 min. Some morphological differences can be observed within the spatial resolution between the two samples, being the oxidized one more brittle with fibers' damages and breaks.

In Fig. 4C the normalized fluorescence spectra measured under excitation at λ_{exc} = 550 nm are shown (measured as average fluorescence intensity from whole the image). Due to the complexity of the sample in terms of fibers density and homogeneity, the spectra were normalized for the fluorescence intensity, and analyzed in terms of band position and shape. In particular, the spectrum of Carbotrace 680 bound to the untreated paper shows a maximum position at 655 nm, which is blue-shifted with respect to 635 nm in the oxidized sample. Also, in the fluorescence spectrum from the oxidized sample, a narrowing of the fluorescence band was observed as well, with respect to the untreated paper possibly indicating a more rigid environment in the dye surroundings.

This hypothesis can be rationalized by taking into account that the oxidation reaction on cellulose polymeric chains is known to occur at the hydroxyl groups on C2-C3 positions of the anhydroglucose units, and leads to the conversion of such hydroxyl groups into aldehyde carbonyls, as herein confirmed by the TTC assay in Fig. 2. The resulting dialdehyde structure is less polar than the untreated cellulose structure.

These measurements suggest that Carbotrace 680 fluorescence is sensitive to paper changes induced by oxidation, and may be useful as a marker for paper oxidation processes.

Paper samples stained with Carbotrace 680 were also studied by using the FLIM technique. The fluorescence lifetime images obtained by the FLIM analysis of the paper samples, along with the corresponding lifetime decays and distributions were acquired (Fig. S3). Then, the data obtained were analyzed by means of the phasor approach. This approach is advantageous as it enabled to analyze the FLIM data and rationalize the observed changes in fluorescence lifetime upon paper oxidation through a standard model-free method, thus avoiding the complex fitting process and user-dependent mathematical procedures. [50]

Firstly, the untreated pure cellulose paper was compared with the paper oxidized for 1440 min (24 h), and the results are reported in Fig. 5. Representative fluorescence intensity images for the two samples are reported in Fig. 5A-B. The corresponding phasor plot is shown in Fig. 5C. Briefly, the model-free phasor approach converts the signal from each pixel of a FLIM image to a point on a semi-circular polar plot called the *universal circle*. The position of the phasors on the universal circle is related to the lifetime of the fluorescence signal, and single-exponential decays lie on the semi-circle while multiple-exponential decays place within the semi-circle. In the case of paper before and after the oxidation, stained with Carbotrace 680, the phasor plot shows two well-separated clouds of pixels corresponding to distinguishable lifetime distributions. Also, fluorescence lifetime distributions are found to lie inside the universal circle indicating that measured lifetimes are characterized by non-single exponential decays. [41] Interestingly, the measurements of Carbotrace 680 lifetime are clearly distinguishable for oxidized and untreated paper. This result suggests the possibility of

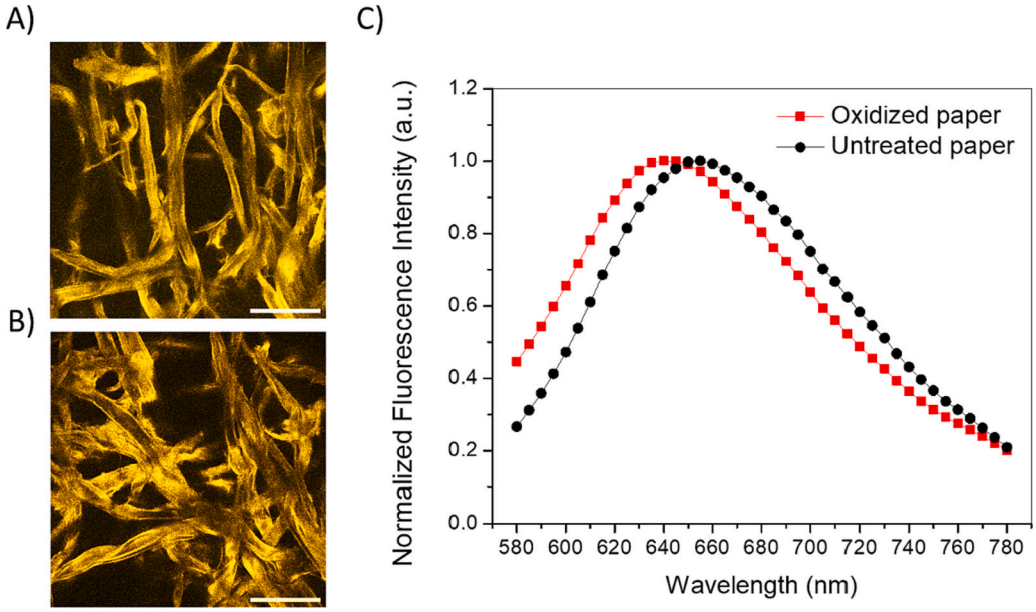

Fig. 4. 1024 × 1024 fluorescence confocal microscopy images of A) before and B) after 1440 min incubation in 15 mM aqueous KIO_4 (scale bars 100 μm); C) Fluorescence spectra of Carbotrace 680 bound on the paper fibers before (black) and after 1440 min of oxidation (red) obtained by using λ_{exc} = 550 nm, acquisition the range 580–780 nm and normalized at the intensity maximum.

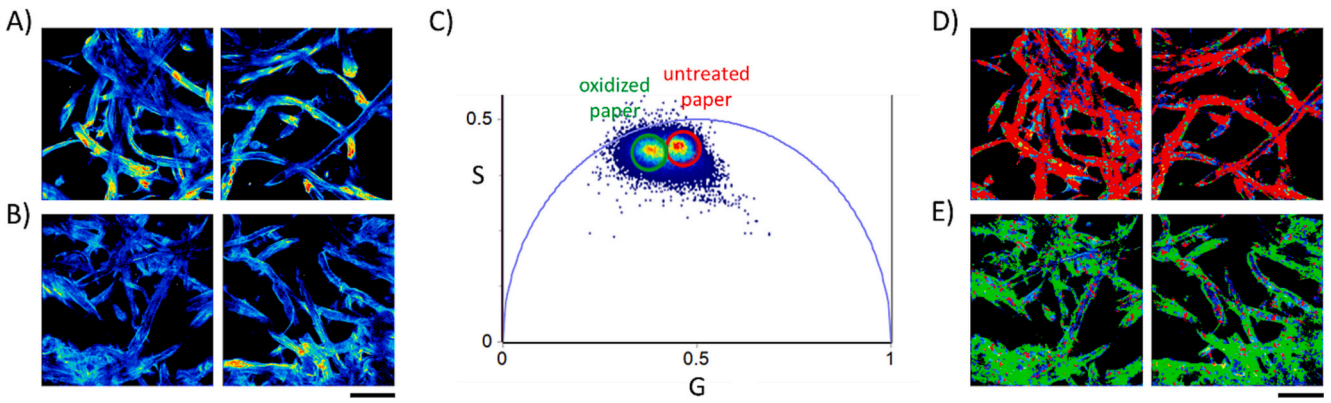

Fig. 5. Phasor analysis of 256 × 256 pixels FLIM measurements on untreated and paper oxidized for 1440 min (24 h). Fluorescence intensity images of A) untreated and B) oxidized paper stained with Carbotrace 680 (intensity scale from blue to red); C) phasor plot obtained from measurements in A and B; D-E) phasor color maps, where each pixel is colored according to the corresponding cursors in the phasor plot (red and green, for untreated and oxidized paper, respectively). The choice of the size and the position of the circles is arbitrary, and it is used to highlight properties of the lifetime distributions. Scale bars are 100 μm.

using Carbotrace 680 dye combined with the FLIM technique as an alternative strategy to distinguish untreated and oxidized pure cellulose paper by lifetime measurements.

In addition, phasor-FLIM measurements are of simple and quite fast acquisition and provide spatial information together with spectral properties of the dye at pixel resolution, which can be translated into information on changes at the molecular level occurring in the sample. Indeed, the phasor-FLIM method enables to easily obtain lifetime maps. By selecting the lifetime distributions on the phasor plot using two colored cursors (red and green in Fig. 5C) the corresponding pixels in the image appear colored with the same color code on the phasor maps in Fig. 5D-E. Such images show the spatial distribution of the lifetimes in the paper samples revealing some heterogeneities of the fluorescence lifetime between the inner and the external parts of the paper fiber.

To obtain more information about the paper fibers oxidation, the oxidation kinetics was investigated in more detail. In the following paper oxidation kinetics was studied from the beginning of the reaction till to the last analyzed oxidation time of 1440 min (24 h). The results shown in Fig. 6 report the phasor analysis of FLIM measurements on Carbotrace 680 stained cellulose paper oxidized for 0, 30, 60, and 1440 min. In Fig. 6A, representative fluorescence intensity images and the corresponding phasor plots are shown for each time point, and their superimposition is reported in Fig. 6B. The cloud-like distributions of lifetime for each oxidation time can be easily distinguished on the phasor plot. For samples at the initial stages of the treatment (30 and 60 min) larger lifetime distributions are found, this being likely due to the heterogeneity of the environment sensed by the dye. The most critical changes are clearly observed at the beginning of the process. After 30 min of paper oxidation, the phasor position shifts towards shorter lifetimes. Then, for more oxidized samples, the phasor shifts back to longer lifetimes. Interestingly, paper samples oxidized at different times up to 1440 min (24 h) exhibit clearly different signals in terms of fluorescence lifetime.

The oxidation treatment induces the reduction of Carbotrace 680

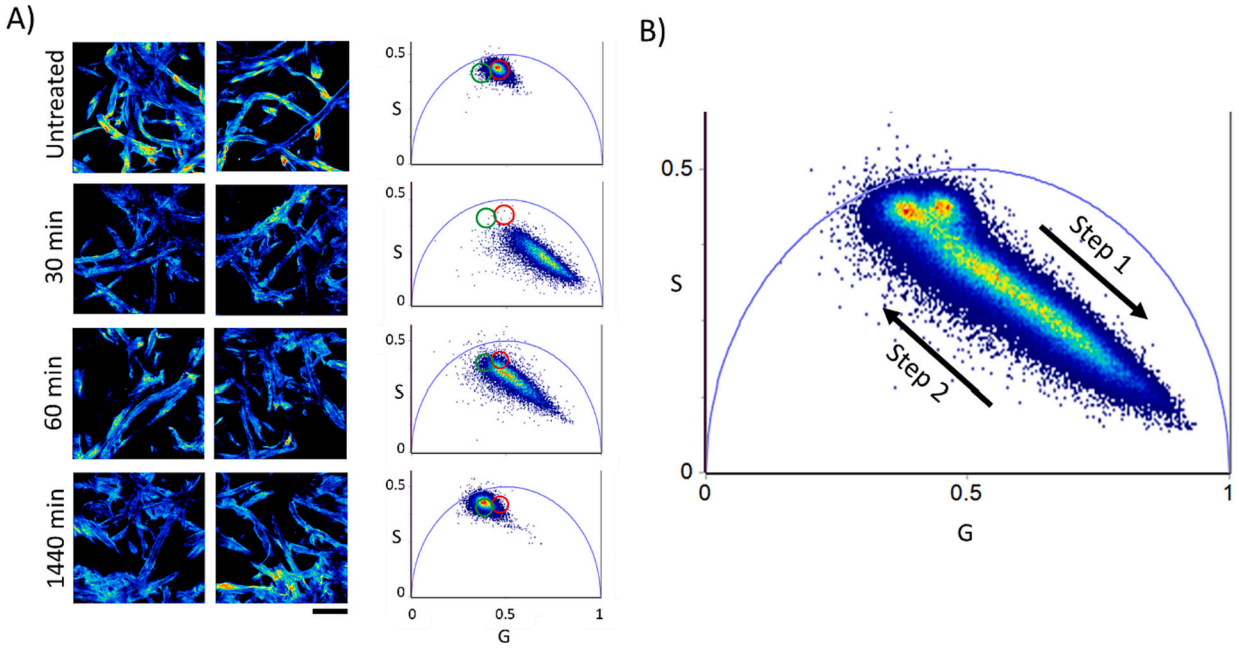

Fig. 6. Phasor analysis of paper oxidation kinetics: A) Fluorescence intensity images of paper at oxidation times 0, 30, 60 and 1440 min (scale bar 100 μm) along with corresponding phasor plots (red and green cursors are centered on the initial and final state lifetime distribution as an eye-guide to highlight phasor changes during the oxidation process), and B) phasor plot of the complete kinetics as a function of the oxidation time the arrows indicate time direction (step 0 from 1 to 30 min, step 2 from 60 min to the end of the process).

lifetime within 30 min of treatment, indicating that when the paper is soaked in the KIO_4 solution the paper fibers change their structures. Such critical modification, which may arise from modifications in the rate of non-radiative decay processes, may stem from the compaction of the dye environment, formation of new interactions with the fibers and so on, observed simultaneously with the growth of crystallinity indexes estimated from XRD and ATR-FTIR measurements (Fig. 3). In the later stages, further modifications occur that are reflected by the increase of lifetime towards a new stable value which is different from the one for the untreated paper. In the last stages, paper fibers undergo partial loss of crystalline structure also at the more packed crystallites moieties, resulting in a longer Carbotrace 680 lifetime. This kind of changes in fluorescence lifetime in dependence on the structural rearrangements of the environment was also observed for other widely used fluorescent dyes. [41,68]

Therefore, the phasor-FLIM approach demonstrated to be a suitable method for the investigation of the paper oxidation process also for the analysis of the changes occurring at the beginning of cellulose oxidation. The analysis of pure cellulose paper oxidation by measurements of Carbotrace 680 lifetime revealed for the dye lifetime a trend analogous to the herein reported crystallinity parameters calculated from XRD and ATR-FTIR data (Fig. 3). A non-linear process in the first hour of paper oxidation was confirmed by the phasor-FLIM analysis. These results contribute to support the idea that pure cellulose paper undergoes a two-step mechanism of oxidation during the Malaprade reaction: in the first step amorphous portions of the cellulose fibers are oxidized and likely depolymerized through the oxidation reaction, then in the second step the more packed crystalline moieties start to be chemically modified, as well.

Moreover, the microscopy-based approach of FLIM provides additional information about the spatial distribution of the dye lifetime on the paper fibers. In this case, this represents a relevant point in order to image at the microscale the oxidation degree of the different parts of the paper fibers during the ageing process. In Fig. 7, a semi-quantitative analysis of the paper fibers oxidation kinetics at 30, 60, and 1440 min is reported. As shown in the phasor plot in Fig. 7A, the observed lifetime changes lie on a straight line allowing the use of a double exponential decay for an empirical description of the observed changes in two main components identified by the green (pure fast component of 0.10 ns) and the red cursor (pure slow component 2.94 ns) in the phasor plot. This procedure is only aimed at producing a lifetime map at pixel resolution where the faster lifetime component is assigned to the lower level of molecular modifications, here attributed to cellulose oxidation, and the slower component to the higher level. Then, a quantitative analysis of lifetime data can be carried out by drawing a straight line where the lifetime distributions lie to connect the two lifetimes' components. This FLIM analysis is based on the decomposition of the phasor plot data using these two principal lifetime components identified via the intersection of the straight line with the universal circle, passing through the lifetime distribution cloud. [41] In Fig. 7B-C, the images used for this analysis are shown in false colors according to the fraction of each lifetime component. The scale goes from blue (lower lifetime) to red (longer lifetime). This color scale, which represents the differences in terms of Carbotrace 680 fluorescence lifetime on the cellulose fibers, can be related to the oxidation degree of the different parts of the paper substrates. For each sample, it is possible to catch changes in the lifetime fraction maps from the different portions of the cellulose fibers. In fact, the phasor-FLIM analysis enabled to clearly visualize a faster change in terms of lifetime for the outer portions of the fibers, that are depicted in yellow and reddish (longer lifetimes) already after 30 min of oxidation, while the inner part of the fibers is still blue (shorter lifetimes). As the oxidation process continues on, the detected lifetime increases in the whole fibers up to an almost homogeneous long lifetime at 1440 min (red pixels). Then, it is possible to assume that the color scale of the sample can be considered a map of the oxidation degree for the different portions of the paper fibers, allowing a clearly spatial visualization of the oxidation process at the microscale.

Therefore, a global view of the microscopy-based analysis of paper fibers oxidation highlighted that after the oxidation process is started, it is possible to visualize in the lifetime fraction maps that molecular modifications due to the oxidizing agent firstly occur at the exterior portions of the cellulose fibers which are likely the more exposed to the solvent, while the fiber interior undergo modification at later stages, highlighting the spatial heterogeneity of the process at the microscale.

4. Conclusions

In the present work, the oxidation of paper constituted of pure cellulose was investigated in detail by means of the FLIM–phasor approach. The herein reported FLIM-phasor approach represents a model-free and advantageous method to follow the paper oxidation process. To set the FLIM-phasor approach, the dye Carbotrace 680 was selected as a suitable fluorescent reporter of the modifications occurring at the cellulose fibers upon accelerated ageing induced by the Malaprade reaction.

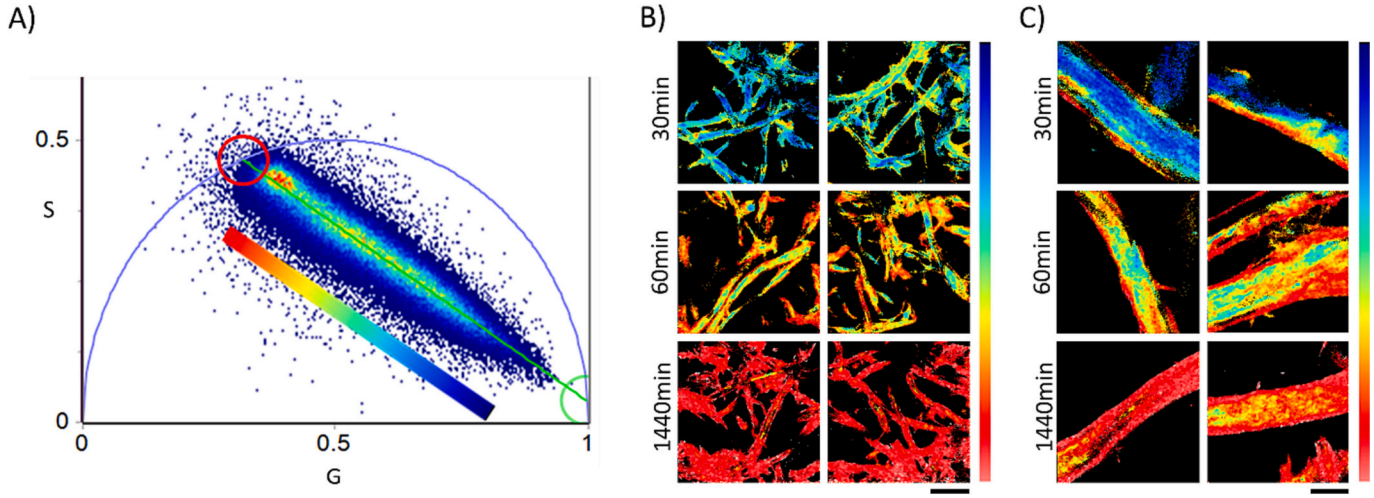

Fig. 7. Component analysis of the phasors from paper oxidation kinetics at 30, 60 and 1440 min: A) phasor plot showing the pure fast component (green cursor) and the pure slower component (red cursor) and the change of the Carbotrace 680 lifetime during the oxidation process; B-C) Lifetime fraction maps of 256 × 256 pixel FLIM images of paper fibers (scale bars are 100 μm and 20 μm in B and C, respectively) obtained from the phasor plot in A. Fluorescence lifetime is represented in a color scale from blue (pure fast component of 0.10 ns) to red (pure slow component at 2.94 ns).

Carbotrace 680 is a recently reported small molecule chosen for its high selectivity in binding polysaccharides structures and the absence of fluorescence as free molecule in water. The staining of paper with Carbotrace 680 is advantageous as carried out by a simple physisorption protocol in an aqueous environment, with no need of further purification protocol as the unbound dye is nonfluorescent in water. Also, labelling paper cellulose with Carbotrace 680 avoids the need to use the carbonyl groups as oxidation maskers, overcoming limitations due to the partial masking of carbonyls as hemiacetals through crosslinking mechanisms. Using the FLIM-phasor approach, spectral properties of Carbotrace 680 were found to show critical differences, both in terms of fluorescence band shape and position as well as in lifetime, in dependence on the oxidation degree of the stained paper. These data suggest that Carbotrace 680 can be applied as a suitable reporter for paper ageing, as its fluorescence properties can be related to modifications of the cellulose fibers at the molecular level.

The results obtained for the first time by the herein reported method were compared with data from typically applied techniques, such as TTC assay, XRD, and ATR-FTIR. The comparative analysis of kinetic data from the applied investigation techniques confirmed a two-step mechanism of oxidation for pure cellulose samples. This observation was already reported in literature, and explained as a consequence of the semi-crystalline nature of cellulose. Indeed, the amorphous portion of the cellulose is firstly involved in the oxidation process, then in the second part of the kinetics the more packed crystallites were oxidized, as well.

In addition, the use of a microscopy-based technique such as FLIM, showed relevant potentiality to investigate paper ageing, since it enabled obtaining spatial information about the paper fibers oxidation. Interestingly, the paper fibers undergo oxidation in a non-uniform way, with the outer portions of the fiber oxidized at the beginning of the process, followed by a complete oxidation of the fiber also in the inner part within 24 h.

In conclusion, the reported phasor-FLIM method is evaluable as an effective and easy to apply strategy to monitor oxidation reactions on cellulose and cellulose-based materials. This represents an interesting point in many research fields, ranging from the analyses of ancient paper artefacts to the monitoring and control of oxidation reactions for cellulose modification towards the design of innovative materials.

Ethics approval and consent to participate

Not applicable.

Consent for publication

Not applicable.

Fundings

This work received funding from European Union (NextGeneration EU), through the MUR-PNRR project SAMOTHRACE (ECS00000022), from MIUR PON AIM1809078-1, and FFR Unipa 2023.

CRediT authorship contribution statement

Vittorio Ferrara: Conceptualization, Data curation, Formal analysis, Methodology, Visualization, Writing – original draft, Writing – review & editing. **Valeria Vetri:** Conceptualization, Funding acquisition, Project administration, Supervision, Writing – review & editing. **Bruno Pignataro:** Writing – review & editing. **Delia Francesca Chillura Martino:** Conceptualization, Funding acquisition, Methodology, Project administration, Writing – review & editing. **Giuseppe Sancataldo:** Conceptualization, Data curation, Formal analysis, Investigation, Methodology, Supervision, Writing – original draft, Writing – review & editing.

Declaration of competing interest

The authors declare that they have no competing interests.

Data availability

The datasets used and/or analyzed during the current study are available from the corresponding authors upon reasonable request.

Acknowledgments

The Advanced Technologies Network (ATeN) Center (University of Palermo) is acknowledged for its infrastructures.

Appendix A. Supplementary data

Supplementary data to this article can be found online at https://doi.org/10.1016/j.ijbiomac.2024.129452.

References

[1] J.A. Heredia-Guerrero, J.J. Benítez, P. Cataldi, U.C. Paul, M. Contardi, R. Cingolani, I.S. Bayer, A. Heredia, A. Athanassiou, All-natural sustainable packaging materials inspired by plant cuticles, Adv Sustain Syst 1 (2017) 1600024, https://doi.org/10.1002/adsu.201600024.
[2] P. Jusner, E. Schwaiger, A. Potthast, T. Rosenau, Thermal stability of cellulose insulation in electrical power transformers – a review, Carbohydr. Polym. 252 (2021) 117196, https://doi.org/10.1016/j.carbpol.2020.117196.
[3] Y.H. Ngo, D. Li, G.P. Simon, G. Garnier, Paper surfaces functionalized by nanoparticles, Adv. Colloid Interface Sci. 163 (2011) 23–38, https://doi.org/10.1016/j.cis.2011.01.004.
[4] M. Bicchieri, A. Sodo, Alcoholic deacidification and simultaneous deacidification-reduction of paper evaluated after artificial and natural aging, J. Cult. Herit. 20 (2016) 599–606, https://doi.org/10.1016/j.culher.2016.02.008.
[5] T. Łojewski, K. Zięba, A. Knapik, J. Bagniuk, A. Lubańska, J. Łojewska, Evaluating paper degradation progress. Cross-linking between chromatographic, spectroscopic and chemical results, Appl. Phys. A Mater. Sci. Process. 100 (2010) 809–821, https://doi.org/10.1007/s00339-010-5657-5.
[6] D. Klemm, B. Heublein, H.P. Fink, A. Bohn, Cellulose: fascinating biopolymer and sustainable raw material, Angew Chemie-Int Ed 44 (2005) 3358–3393, https://doi.org/10.1002/anie.200460587.
[7] J. Credou, T. Berthelot, Cellulose: from biocompatible to bioactive material, J. Mater. Chem. B 2 (2014) 4767–4788, https://doi.org/10.1039/c4tb00431k.
[8] S. Acharya, Y. Hu, H. Moussa, N. Abidi, Preparation and characterization of transparent cellulose films using an improved cellulose dissolution process, J. Appl. Polym. Sci. 134 (2017) 1–12, https://doi.org/10.1002/app.44871.
[9] Z. Peter, Order in cellulosics: historical review of crystal structure research on cellulose, Carbohydr. Polym. 254 (2021) 117417, https://doi.org/10.1016/j.carbpol.2020.117417.
[10] L.J. Gibson, The hierarchical structure and mechanics of plant materials, J. R. Soc. Interface 9 (2012) 2749–2766, https://doi.org/10.1098/rsif.2012.0341.
[11] S. Zervos, I. Alexopoulou, Paper conservation methods: a literature review, Cellulose 22 (2015) 2859–2897, https://doi.org/10.1007/s10570-015-0699-7.
[12] M. Yatagai, S.H. Zeronian, Effect of ultraviolet light and heat on the properties of cotton cellulose, Cellulose 1 (1994) 205–214, https://doi.org/10.1007/BF00813508.
[13] J. Pérez, J. Muñoz-Dorado, T. de la Rubia, J. Martínez, Biodegradation and biological treatments of cellulose, hemicellulose and lignin: an overview, Int. Microbiol. 5 (2002) 53–63, https://doi.org/10.1007/s10123-002-0062-3.
[14] M. Bicchieri, F. Valentini, A. Calcaterra, M. Talamo, Newly developed Nano-calcium carbonate and Nano-calcium Propanoate for the Deacidification of library and archival materials, J. Anal. Methods Chem. 2017 (2017), https://doi.org/10.1155/2017/2372789.
[15] R. Giorgi, L. Dei, M. Ceccato, C. Schettino, P. Baglioni, Nanotechnologies for conservation of cultural heritage: paper and canvas deacidification, Langmuir 18 (2002) 8198–8203, https://doi.org/10.1021/la025964d.
[16] J. Łojewska, P. Miśkowiec, T. Łojewski, L.M. Proniewicz, Cellulose oxidative and hydrolytic degradation: in situ FTIR approach, Polym. Degrad. Stab. 88 (2005) 512–520, https://doi.org/10.1016/j.polymdegradstab. 2004.12.012.
[17] J. Łojewska, A. Lubańska, P. Miśkowiec, T. Łojewski, L.M. Proniewicz, FTIR in situ transmission studies on the kinetics of paper degradation via hydrolytic and oxidative reaction paths, Appl. Phys. A Mater. Sci. Process. 83 (2006) 597–603, https://doi.org/10.1007/s00339-006-3529-9.
[18] S. Bastone, D.F. Chillura Martino, V. Renda, M.L. Saladino, G. Poggi, E. Caponetti, Alcoholic nanolime dispersion obtained by the insolubilisation-precipitation method and its application for the deacidification of ancient paper, Colloids Surfaces A Physicochem Eng Asp 513 (2017) 241–249, https://doi.org/10.1016/j.colsurfa.2016.10.049.
[19] Q. Xu, G. Poggi, C. Resta, M. Baglioni, P. Baglioni, Grafted nanocellulose and alkaline nanoparticles for the strengthening and deacidification of cellulosic

artworks, J. Colloid Interface Sci. 576 (2020) 147–157, https://doi.org/10.1016/j.jcis.2020.05.018.
[20] I. Natali, M.L. Saladino, F. Andriulo, D. Chillura Martino, E. Caponetti, E. Carretti, L. Dei, Consolidation and protection by nanolime: recent advances for the conservation of the graffiti, Carceri dello Steri Palermo and of the 18th century lunettes, SS. Giuda e Simone cloister, Corniola (Empoli), J Cult Herit 15 (2014) 151–158, https://doi.org/10.1016/j.culher.2013.03.002.
[21] M. Cocca, L. D'Arienzo, L. D'Orazio, Effects of different artificial agings on structure and properties of Whatman paper samples, ISRN Mater. Sci. 2011 (2011) 1–7, https://doi.org/10.5402/2011/863083.
[22] B. Sun, Q. Hou, Z. Liu, Y. Ni, Sodium periodate oxidation of cellulose nanocrystal and its application as a paper wet strength additive, Cellulose 22 (2015) 1135–1146, https://doi.org/10.1007/s10570-015-0575-5.
[23] S. Coseri, G. Biliuta, L.F. Zemljič, J.S. Srndovic, P.T. Larsson, S. Strnad, T. Kreže, A. Naderi, T. Lindström, One-shot carboxylation of microcrystalline cellulose in the presence of nitroxyl radicals and sodium periodate, RSC Adv. 5 (2015) 85889–85897, https://doi.org/10.1039/C5RA16183E.
[24] A. Potthast, M. Kostic, S. Schiehser, P. Kosma, T. Rosenau, Studies on oxidative modifications of cellulose in the periodate system: molecular weight distribution and carbonyl group profiles, Holzforschung 61 (2007) 662–667, https://doi.org/10.1515/HF.2007.099.
[25] A.S. Perlin, Glycol-cleavage oxidation, Adv. Carbohydr. Chem. Biochem. 60 (2006) 183–250, https://doi.org/10.1016/S0065-2318(06)60005-X.
[26] M. Strlič, B. Pihlar, Determination of reducing carbonyl groups in cellulose in the solvent system LiCl/N, N-dimethylacetamide, Fresenius J. Anal. Chem. 357 (1997) 670–675, https://doi.org/10.1007/s002160050232.
[27] S. Park, D.K. Johnson, C.I. Ishizawa, P.A. Parilla, M.F. Davis, Measuring the crystallinity index of cellulose by solid state 13C nuclear magnetic resonance, Cellulose 16 (2009) 641–647, https://doi.org/10.1007/s10570-009-9321-1.
[28] S. Park, J.O. Baker, M.E. Himmel, P.A. Parilla, D.K. Johnson, Cellulose crystallinity index: measurement techniques and their impact on interpreting cellulase performance, Biotechnol. Biofuels 3 (2010) 1–10, https://doi.org/10.1186/1754-6834-3-10.
[29] Y.H. Xu, C. Huang, Effect of sodium periodate selective oxidation on crystallinity of cotton cellulose, Adv. Mater. Res. 197–198 (2011) 1201–1204, doi:10.4028/www.scientific.net/AMR.197-198.1201.
[30] H. Vu, J.W. Woodcock, A. Krishnamurthy, J. Obrzut, J.W. Gilman, E.B. Coughlin, Visualization of polymer dynamics in cellulose nanocrystal matrices using fluorescence lifetime measurements, ACS Appl. Mater. Interfaces 14 (2022) 10793–10804, https://doi.org/10.1021/acsami.1c21906.
[31] E. Piacenza, A. Presentato, F. Di Salvo, R. Alduina, V. Ferrara, V. Minore, A. Giannusa, G. Sancataldo, D.F. Chillura Martino, A combined physical–chemical and microbiological approach to unveil the fabrication, provenance, and state of conservation of the Kinkarakawa-gami art, Sci. Rep. 10 (2020) 1–13, https://doi.org/10.1038/s41598-020-73226-6.
[32] P. Wang, G. You, J. Hou, C. Wang, Y. Xu, L. Miao, T. Feng, F. Zhang, Responses of wastewater biofilms to chronic CeO2 nanoparticles exposure: structural, physicochemical and microbial properties and potential mechanism, Water Res. 133 (2018) 208–217, https://doi.org/10.1016/j.watres.2018.01.031.
[33] C.B. Wilda, A. Burnstock, K. Suhling, F. Mattioli Della Rocca, R.K. Henderson, J. Nedbal, Visualising varnish removal for conservation of paintings by fluorescence lifetime imaging (FLIM), Herit Sci 11 (2023) 127, https://doi.org/10.1186/s40494-023-00957-w.
[34] A. Potthast, S. Schiehser, T. Rosenau, M. Kostic, Oxidative modifications of cellulose in the periodate system - reduction and beta-elimination reactions: 2nd ICC 2007, Tokyo, Japan, October 25-29, 2007, Holzforschung 63 (2009) 12–17, https://doi.org/10.1515/HF.2009.108.
[35] A. Potthast, J. Röhrling, T. Rosenau, A. Borgards, H. Sixta, P. Kosma, A novel method for the determination of carbonyl groups in cellulosics by fluorescence labelling. 3. Monitoring oxidative processes, Biomacromolecules 4 (2003) 743–749, https://doi.org/10.1021/bm025759c.
[36] J. Erlandsson, T. Pettersson, T. Ingverud, H. Granberg, P.A. Larsson, M. Malkoch, L. Wågberg, On the mechanism behind freezing-induced chemical crosslinking in ice-templated cellulose nanofibril aerogels, J. Mater. Chem. A 6 (2018) 19371–19380, https://doi.org/10.1039/c8ta06319b.
[37] F.X. Choong, L. Lantz, H. Shirani, A. Schulz, K.P.R. Nilsson, U. Edlund, A. Richter-Dahlfors, Stereochemical identification of glucans by a donor–acceptor–donor conjugated pentamer enables multi-carbohydrate anatomical mapping in plant tissues, Cellulose 26 (2019) 4253–4264, https://doi.org/10.1007/s10570-019-02381-5.
[38] J.R. Lakowicz, Principles of Fluorescence Spectroscopy, 2006.
[39] G. Sancataldo, G. Avellone, V. Vetri, Nile red lifetime reveals microplastic identity, Environ Sci Process Impacts 22 (2020) 2266–2275, https://doi.org/10.1039/D0EM00348D.
[40] S. Anselmo, G. De Luca, V. Ferrara, B. Pignataro, G. Sancataldo, V. Vetri, Insight into mechanisms of creatinine optical sensing using fluorescein-gold complex, Methods Appl Fluoresc 10 (2022), https://doi.org/10.1088/2050-6120/ac8524.
[41] S. Anselmo, G. Sancataldo, H. Mørck Nielsen, V. Foderà, V. Vetri, Peptide–membrane interactions monitored by fluorescence lifetime imaging: a study case of transportan 10, Langmuir 37 (2021) 13148–13159, https://doi.org/10.1021/acs.langmuir.1c02392.
[42] R. Datta, T.M. Heaster, J.T. Sharick, A.A. Gillette, M.C. Skala, Fluorescence lifetime imaging microscopy: fundamentals and advances in instrumentation, analysis, and applications, J. Biomed. Opt. 25 (2020) 71203, https://doi.org/10.1117/1.JBO.25.7.071203.
[43] K. Suhling, L.M. Hirvonen, J.A. Levitt, P.H. Chung, C. Tregidgo, A. Le Marois, D. A. Rusakov, K. Zheng, S. Ameer-Beg, S. Poland, S. Coelho, R. Henderson, N. Krstajic, Fluorescence lifetime imaging (FLIM): basic concepts and some recent developments, Med Photonics 27 (2015) 3–40, https://doi.org/10.1016/j.medpho.2014.12.001.
[44] W. Becker, Fluorescence lifetime imaging – techniques and applications, J. Microsc. 247 (2012) 119–136, https://doi.org/10.1111/j.1365-2818.2012.03618.x.
[45] M.Y. Berezin, S. Achilefu, Fluorescence lifetime measurements and biological imaging, Chem. Rev. 110 (2010) 2641–2684, https://doi.org/10.1021/cr900343z.
[46] J.W. Borst, A.J.W.G. Visser, Fluorescence lifetime imaging microscopy in life sciences, Meas. Sci. Technol. 21 (2010) 102002, https://doi.org/10.1088/0957-0233/21/10/102002.
[47] S. Ameer-Beg, K. Suhling, M. Kuimova, Special issue on fluorescence lifetime imaging (FLIM): from fundamentals to applications, Methods Appl Fluoresc 8 (2020) 40401, https://doi.org/10.1088/2050-6120/abad19.
[48] C. Stringari, A. Cinquin, O. Cinquin, M.A. Digman, P.J. Donovan, E. Gratton, Phasor approach to fluorescence lifetime microscopy distinguishes different metabolic states of germ cells in a live tissue, Proc. Natl. Acad. Sci. 108 (2011) 13582–13587, https://doi.org/10.1073/pnas.1108161108.
[49] G. De Luca, D. Fennema Galparsoro, G. Sancataldo, M. Leone, V. Foderà, V. Vetri, Probing ensemble polymorphism and single aggregate structural heterogeneity in insulin amyloid self-assembly, J. Colloid Interface Sci. 574 (2020) 229–240, https://doi.org/10.1016/j.jcis.2020.03.107.
[50] S. Ranjit, L. Malacrida, D.M. Jameson, E. Gratton, Fit-free analysis of fluorescence lifetime imaging data using the phasor approach, Nat. Protoc. 13 (2018) 1979–2004, https://doi.org/10.1038/s41596-018-0026-5.
[51] L. Malacrida, S. Ranjit, D.M. Jameson, E. Gratton, The phasor plot: a universal circle to Advance fluorescence lifetime analysis and interpretation, Annu. Rev. Biophys. 50 (2021) 575–593, https://doi.org/10.1146/annurev-biophys-062920-063631.
[52] M.A. Digman, V.R. Caiolfa, M. Zamai, E. Gratton, The phasor approach to fluorescence lifetime imaging analysis, Biophys. J. 94 (2008) L14–L16, https://doi.org/10.1529/biophysj.107.120154.
[53] S. Margutti, G. Conio, P. Calvini, E. Pedemonte, Hydrolytic and oxidative degradation of paper, Restaurator 22 (2001) 67–83, https://doi.org/10.1515/REST.2001.67.
[54] F. Coppola, A. Modelli, Oxidative degradation of non-recycled and recycled paper, Cellulose 27 (2020) 8977–8987, https://doi.org/10.1007/s10570-020-03395-0.
[55] E.R. Neves, S. Schäfer, A. Phillips, J. Canejo, M.F. Macedo, Antifungal effect of different methyl and propyl paraben mixtures on the treatment of paper biodeterioration, Int. Biodeter. Biodegr. 63 (2009) 267–272, https://doi.org/10.1016/j.ibiod.2008.07.011.
[56] C. Vibert, B. Fayolle, D. Ricard, A.-L. Dupont, Decoupling hydrolysis and oxidation of cellulose in permanent paper aged under atmospheric conditions, Carbohydr. Polym. 310 (2023) 120727, https://doi.org/10.1016/j.carbpol.2023.120727.
[57] S.Y. Oh, Yoo D. Il, Y. Shin, H.C. Kim, H.Y. Kim, Y.S. Chung, W.H. Park, J.H. Youk, Crystalline structure analysis of cellulose treated with sodium hydroxide and carbon dioxide by means of X-ray diffraction and FTIR spectroscopy, Carbohydr. Res. 340 (2005) 2376–2391, https://doi.org/10.1016/j.carres.2005.08.007.
[58] A. Thygesen, J. Oddershede, H. Lilholt, A.B. Thomsen, K. Ståhl, On the determination of crystallinity and cellulose content in plant fibres, Cellulose 12 (2005) 563–576, https://doi.org/10.1007/s10570-005-9001-8.
[59] M.N. Costa, B. Veigas, J.M. Jacob, D.S. Santos, J. Gomes, P.V. Baptista, R. Martins, J. Inácio, E. Fortunato, A low cost, safe, disposable, rapid and self-sustainable paper-based platform for diagnostic testing: lab-on-paper, Nanotechnology 25 (2014), https://doi.org/10.1088/0957-4484/25/9/094006.
[60] D. Lourdin, J. Peixinho, J. Bréard, B. Cathala, E. Leroy, B. Duchemin, Concentration driven cocrystallisation and percolation in all-cellulose nanocomposites, Cellulose 23 (2016) 529–543, https://doi.org/10.1007/s10570-015-0805-x.
[61] J. Široký, R.S. Blackburn, T. Bechtold, J. Taylor, P. White, Attenuated total reflectance Fourier-transform infrared spectroscopy analysis of crystallinity changes in lyocell following continuous treatment with sodium hydroxide, Cellulose 17 (2010) 103–115, https://doi.org/10.1007/s10570-009-9378-x.
[62] T. Auxenfans, D. Crônier, B. Chabbert, G. Paës, Understanding the structural and chemical changes of plant biomass following steam explosion pretreatment, Biotechnol. Biofuels 10 (2017) 36, https://doi.org/10.1186/s13068-017-0718-z.
[63] F. Carrillo, X. Colom, J.J. Suñol, J. Saurina, Structural FTIR analysis and thermal characterisation of lyocell and viscose-type fibres, Eur. Polym. J. 40 (2004) 2229–2234, https://doi.org/10.1016/j.eurpolymj.2004.05.003.
[64] M.L. Nelson, R.T. O'Connor, Relation of certain infrared bands to cellulose crystallinity and crystal lattice type. Part II. A new infrared ratio for estimation of crystallinity in celluloses I and II, J. Appl. Polym. Sci. 8 (1964) 1325–1341, https://doi.org/10.1002/app.1964.070080323.
[65] S.Y. Oh, Yoo D. Il, Y. Shin, G. Seo, FTIR analysis of cellulose treated with sodium hydroxide and carbon dioxide, Carbohydr. Res. 340 (2005) 417–428, https://doi.org/10.1016/j.carres.2004.11.027.
[66] G. Sancataldo, S. Anselmo, V. Vetri, Phasor-FLIM analysis of Thioflavin T self-quenching in Concanavalin amyloid fibrils, Microsc. Res. Tech. 83 (2020) 811–816, https://doi.org/10.1002/jemt.23472.
[67] M.L. Barcellona, E. Gratton, The fluorescence properties of a DNA probe, Eur. Biophys. J. 17 (1990) 315–323, https://doi.org/10.1007/BF00258380.
[68] E. Rao, V. Foderà, M. Leone, V. Vetri, Direct observation of alpha-lactalbumin, adsorption and incorporation into lipid membrane and formation of lipid/protein

hybrid structures, Biochim Biophys Acta-Gen Subj 1863 (2019) 784–794, https://doi.org/10.1016/j.bbagen.2019.02.005.